Interstitial oxygen in germanium and silicon

Emilio Artacho and Félix Ynduráin
Instituto Nicolás Cabrera and Departamento de Física de la Materia Condensada, C-III Universidad Autónoma de Madrid, 28049 Madrid, Spain

Bernard Pajot
Groupe de Physique des Solides (Unité Associée au CNRS), Tour 23, Université Denis Diderot, 2 Place Jussieu, 75251 Paris Cedex 05, France

Rafael Ramírez and Carlos P. Herrero
Instituto de Ciencia de Materiales, Consejo Superior de Investigaciones Científicas, Cantoblanco, 28049 Madrid, Spain

Ludmila I. Khirunenko
Institute of Physics, National Academy of Sciences of Ukraine, Prospect Nauki 46, 252650 Kiev 22, Ukraine

Kohei M. Itoh
Department of Applied Physics and Physico-Informatics, Keio University, 3-14-1 Hiyoshi, Kohoku-ku, Yokohama 223, Japan

Eugene E. Haller
Lawrence Berkeley National Laboratory and University of California, Berkeley, California 94720
(Received 25 February 1997)

The microscopic structure of interstitial oxygen in germanium and its associated dynamics are studied both experimentally and theoretically. The infrared absorption spectrum is calculated with a dynamical matrix model based on first-principles total-energy calculations describing the potential energy for the nuclear motions. Spectral features and isotope shifts are calculated and compared with available experimental results. From new spectroscopic data on natural and on quasimonoisotopic germanium samples, new isotope shifts have been obtained and compared with the theoretical predictions. The low-energy spectrum is analyzed in terms of a hindered rotor model. A fair understanding of the center is achieved, which is then compared with interstitial oxygen in silicon. The oxygen atom is nontrivially quantum delocalized both in silicon and in germanium, but the physics is shown to be very different: while the Si-O-Si quasimolecule is essentially linear, the Ge-O-Ge structure is puckered. The delocalization in a highly anharmonic potential well of oxygen in silicon is addressed using path-integral Monte Carlo simulations, for comparison with the oxygen rotation in germanium. The understanding achieved with this new information allows us to explain the striking differences between both systems, in both the infrared and the far-infrared spectral regions, and the prediction of the existence of hidden vibrational modes, never directly observed experimentally, but soundly supported by the isotope-shift analysis. [S0163-1829(97)08631-1]

I. INTRODUCTION

The understanding of apparently solved old problems is sometimes found to be limited when looking at them in detail. A thorough revision of such a problem, often with newer techniques, reveals a richer physics, and also subtleties that hindered the full understanding of the problem in the past. Interstitial oxygen in covalent semiconductors is one of these problems. Oxygen in silicon has been very thoroughly studied[1] in the past for technological reasons. Oxygen in germanium, while first investigated at about the same time,[2,3] has been reinvestigated more actively recently, due to progress in spectroscopy and to the availability of quasimonoisotopic germanium samples.[4–9] Although the basic structure for the defect centers is generally accepted, namely, atomic oxygen breaking the Si—Si or the Ge—Ge bonds and staying near the bond center, there are some fundamental aspects of these systems that remain unsolved. For example, the comparison of the low-energy-excitation and infrared spectra of both centers is certainly puzzling. The low-energy-excitation spectra of interstitial oxygen in silicon[10] and germanium[6,8] are fundamentally different, showing their characteristic features at different energy scales. The infrared spectra are also different, and they do not quite adapt to the modes of the Si_2O (Refs. 11, 12) or Ge_2O (Ref. 8) pseudomolecules.

The available experimental information is based on absorption spectroscopy, using photons or phonons, in the infrared or far infrared. Early studies on interstitial oxygen in silicon ($Si:O_i$) showed two main absorption features in the infrared[1] (519 cm^{-1} and 1136 cm^{-1}) and another structure in the far infrared[10] (29 cm^{-1}). The three main features were associated with the three fundamental vibrational modes of a puckered Si_2O molecule, ν_1 (the 519 cm^{-1} peak), ν_2 (the 29 cm^{-1} band), and ν_3 (the 1136 cm^{-1} or 9 μm stretching band), as displayed in Fig. 1(a). The analysis of the fine

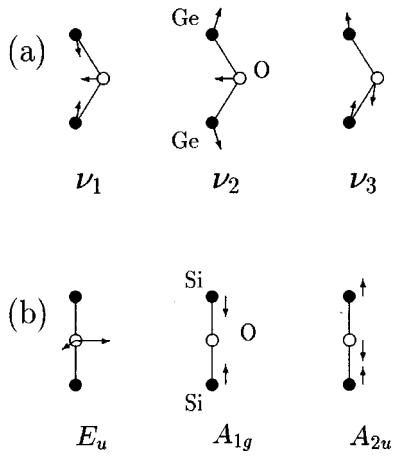

FIG. 1. Fundamental vibrational modes of (a) the puckered Ge_2O and (b) the linear Si_2O quasimolecules. The traditional nomenclature has been adopted for Ge_2O. For Si_2O the nomenclature corresponds to the D_{3d} point group, appropriate for the linear structure.

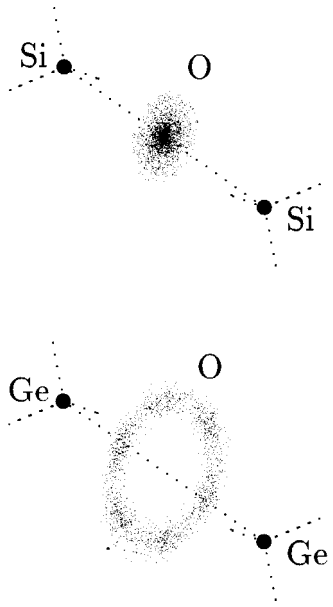

FIG. 2. Quantum delocalization of oxygen in Si:O_i and Ge:O_i, in the plane perpendicular to the Si-Si (Ge-Ge) axis.

structure of the high- and low-frequency features[10] offered insight into the nature of the microscopic structure of the center and the oxygen dynamics. In spite of the correctness and merit of this analysis,[10] it was only recently shown[11,12] that the puckered image was misleading, a better one being that of a linear $Si_3{\equiv}SiOSi{\equiv}Si_3$ molecule with dynamic D_{3d} symmetry, as shown in Fig. 2 [see Fig. 1(b) for the vibration modes]. The assignments were consequently revised: the 519 cm^{-1} peak is not a vibration of the Si_2O pseudomolecule (not shown in Fig. 1), but a backbond Si—Si vibration of E_u symmetry of the corresponding D_{3d} point group. The stretching mode (ν_3) remains essentially unchanged, being of A_{2u} symmetry. The equivalent to the ν_1 mode is an A_{1g} symmetric stretching mode invisible to the infrared, located at around 600 cm^{-1}. The observed combination mode at 1750 cm^{-1} and its isotope shifts[13] strongly support this new model.[14]

Note the difference in mode counting between both geometries. A linear SiOSi structure gives two nondegenerate modes and one doubly degenerate mode, that is, four modes, compared with the three nondegenerate modes for the puckered unit. This is in agreement with the number of vibrational modes of an N-atom molecule, which is $3N-5$ and $3N-6$ for linear and nonlinear molecules, respectively.

In the case of interstitial oxygen in germanium (Ge:O_i), infrared-absorption bands have been reported near 860 and 1270 cm^{-1},[2] which are equivalent to the 1136 and 1750 cm^{-1} bands in Si:O_i. Low-energy absorptions have also been detected by phonon spectroscopy,[6] at a much lower-energy scale than the far-infrared absorption in Si, but there is no report on any feature in the intermediate-frequency range.

In this work we analyze in detail the Ge:O_i center, using both experimental and theoretical information. Also, some new information will be reported for Si:O_i. Both systems are compared throughout this work. Using simple but realistic theoretical tools and new isotope-shift measurements we have reached the following conclusions: (i) Interstitial oxygen is quantum delocalized in both hosts, but this delocalization is essentially different in silicon and in germanium, the difference being graphically depicted in Fig. 2. In the case of germanium the defect can be well accounted for by an elastic, hindered, two-dimensional rotor, whereas in the silicon case oxygen is delocalized around the original silicon-silicon bond center position. (ii) As a consequence of the above, it is meaningless to talk about a static geometry of the defect. (iii) In the Ge:O_i case, the puckered Ge_2O molecule picture holds, the lowest vibrational energy (ν_2) being substantially higher in energy than the observed low-energy structure (purely rotational). (iv) There are infrared inactive (or at least with a weak activity) vibrational modes that were never discussed before. (v) The bonding of oxygen to the Si and in Ge hosts is quite different, as can be deduced from Fig. 2.

The different pieces of information leading to these conclusions are organized as follows. In Sec. II we analyze the experiments in the far-infrared spectral region and, with the help of total-energy and path-integral calculations, we determine the ''equilibrium'' configuration and low-energy dynamics of interstitial oxygen both in silicon and in germanium. In Sec. III, based on the above described atomic configurations, we calculate the atomic vibration and infrared spectra associated with the defects. A detailed comparison with the available experimental data is performed. The results of Sec. III motivate the experimental measurement of isotope shifts in isotopically pure samples. The experiments have been performed and their description and results are presented in Sec. IV. Finally, in Sec. V a summary of the work is given.

II. ATOMIC CONFIGURATION

A. Low-energy excitations

Both Si:O_i and Ge:O_i display spectral features in the far-infrared region that cannot be accounted for by vibrational excitations of the atoms involved. This originates from the deviation from the usual behavior of atoms harmonically vibrating around the absolute minimum of the potential. The oxygen atom is nontrivially delocalized in a wider region of

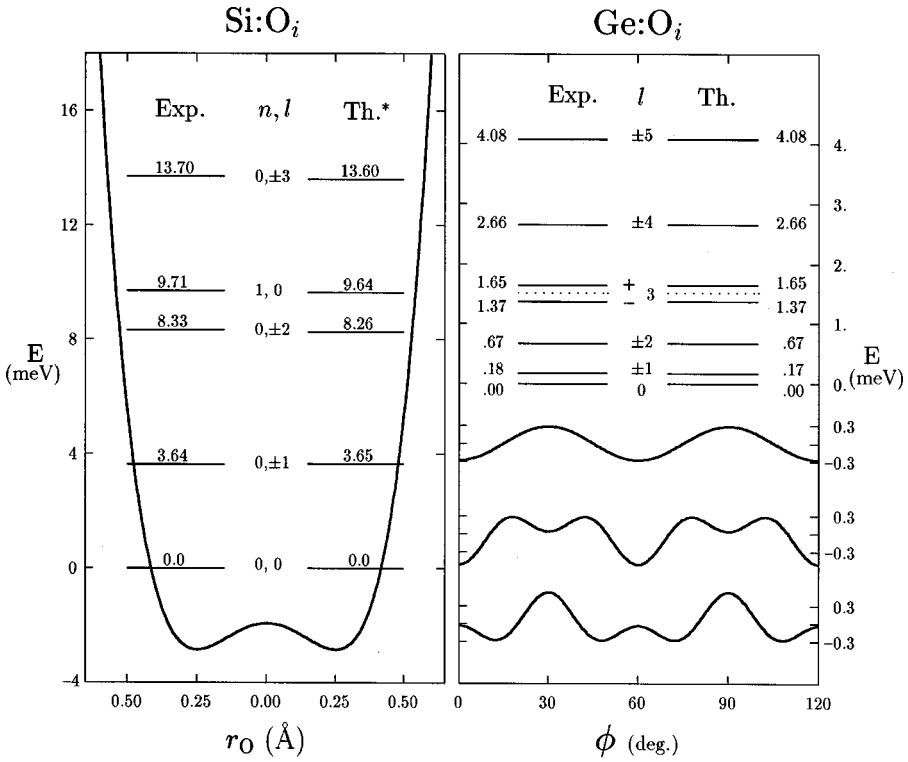

FIG. 3. Low-energy levels of Si:O$_i$ and Ge:O$_i$. For Si:O$_i$ the levels inferred from far-infrared-absorption data (Ref. 10) are compared with the results of the calculations of Yamada-Kaneta, Kaneta, and Ogawa (Ref. 11) based on the anharmonic potential well, coupled to the ν_3 vibration mode. Also displayed is the renormalized potential for the ground state of ν_3. For Ge:O$_i$, the results of phonon spectroscopy of Gienger, Glaser, and Laβmann (Ref. 6) are compared with the results of the hindered rotor model. Also shown are three potentials compatible with the data, differing in the amplitude of the $\cos(12\phi)$ term (zero, negative, or positive, respectively), plotted versus the azimuthal angle ϕ.

space, both in silicon and in germanium. The two centers, however, display important differences both in the energy scale of the low-energy excitations and in the spectral patterns, which are due to the very different character in the delocalization of oxygen in these centers, as illustrated in Fig. 2. This image is supported by the analysis shown in Fig. 3, where the low-energy excitations of both interstitial centers are shown and compared to theoretical models described in the following.

In the case of Si:O$_i$ the energy levels resulting from the far-infrared measurements of Bosomworth *et al.*[10] are displayed in Fig. 3. They were originally explained[10] by considering the oxygen atom moving around the bond-center (BC) position in the plane perpendicular to the original Si-Si axis, in a highly anharmonic potential looking like the base of a wine bottle. The theoretical results displayed in the figure are the ones of Yamada-Kaneta, Kaneta, and Ogawa,[11] who improved the model by including the interaction of these low-energy anharmonic excitations with the high-energy stretching vibration of the center [A_{2u} mode in Fig. 1(b)]. The figure shows the potential for the low-energy oxygen motion obtained from the fit. The ground-state energy being higher than the energy barrier at BC ($r_O=0$) gives rise to the rather unusual situation depicted in Fig. 2, where the oxygen atom is quantum delocalized in the whole well, a large region of space, with maximum probability density at the BC site in spite of the maximum of the potential at that point.[12] This situation is examined in more detail in Sec. II C.

For Ge:O$_i$ the situation is quite different. The levels derived from the phonon spectroscopy results of Gienger, Glaser, and Laβmann[6] are also shown in Fig. 3. The data were originally analyzed[6] in terms of a rigid rotor, the split of the $l=3$ levels being associated to an order-6 azimuthal modulation of the potential. A good agreement with experiments was achieved, except for a deviation for high l values. We have reconsidered the experimental data in terms of a nonrigid rotor model taking into account the centrifugal distortion and higher order hindering potentials. The calculated energy levels are displayed side by side with the experimental ones in Fig. 3.

The Hamiltonian of the model has two terms,

$$H=H_0+H_h. \tag{1}$$

H_0 is the Hamiltonian of a nonrigid (elastic) rotor in two dimensions,[15] which is diagonal in the basis of eigenstates of J_z, the component of the angular momentum perpendicular to the plane of rotation. The eigenvalues of H_0 are[15]

$$E_0^l=Bl^2-Dl^4, \tag{2}$$

with $l=0,1,2\ldots$ being the angular-momentum quantum number for two-dimensional rotation. Except for the ground state ($l=0$), each eigenvalue has two degenerate eigenvectors characterized by the quantum number $m=-l,+l$. The rotor constant B is

$$B=\frac{\hbar^2}{2I}, \tag{3}$$

I being the momentum of inertia. The centrifugal distortion coefficient D is

$$D=\frac{4B^3}{\hbar^2\omega^2}, \tag{4}$$

where ω is the frequency of vibration of the rotor in the radial direction.

H_h is the hindering potential. It is a function of the azimuthal angle ϕ that, because of the symmetry of the center, has to be even $[H_h(\phi)=H_h(-\phi)]$ and periodic with a period of $\pi/3$. It can thus be written as

$$H_h=\sum_{n\geqslant 1} 2a_n\cos(6n\phi), \tag{5}$$

with any shape consistent with the symmetry being describable in terms of the a_n coefficients. The hindering potential will produce the splitting of the degeneracies only for the states with $l=3,6,9,\ldots$ as shown below.

The solution of the model given by H for the desired eigenvalues and eigenvectors to the desired accuracy can be obtained by numerically diagonalizing the matrix of H in the basis of the eigenvectors of H_0. In the ϕ representation, these eigenvectors are

$$\psi_m(\phi)=\frac{1}{\sqrt{2\pi}}\,e^{im\phi}, \tag{6}$$

with $m=0,\pm 1,\pm 2,\ldots$. The matrix for H_h is obtained from

$$\langle m|2a_n\cos(6n\phi)|m'\rangle=a_n\delta_{m,m'\pm 6n}. \tag{7}$$

The infinite matrix for H is constructed from Eqs. (2) and (7). The problem can be solved by diagonalizing the finite matrix obtained for the subset of basis states with angular momentum l smaller than a certain $l_{\max}$. Then, $l_{\max}$ is increased until the considered eigenvalues converge within the desired accuracy. For the results shown in Fig. 3 a value of $l_{\max}$ of the order of 30 is perfectly sufficient.

The different parameters entering the problem affect the eigenvalues in well distinguishable ways. This fact makes the model useful since information can be obtained for a few of them without the inference of the others. A fit of the experimental data, as presented in Fig. 3, can be obtained with just three parameters, B, D, and a_1, independently of the values of higher a_n's. The obtained agreement is remarkable, which supports the picture of Fig. 2.

The spacing of the lower eigenvalues defines the rotor constant as $B=0.175\pm 0.005$ meV, the $\pm$ range indicating the variability of B for different (reasonable) values of the other parameters. This results in $I=11.9$ amu Å^2. Similarly, the splitting of the $l=3$ levels defines the coefficient of the fundamental term of the hindering potential as $|a_1|=0.13\pm 0.02$ meV. The centrifugal distortion term D affects the higher eigenvalues by reducing their spacings. Its value is more sensitive, however, to the other parameters, specifically to a_2. The lack of experimental information for $l>5$ prevents the evaluation of a_2 and coefficients of higher harmonics, since they affect only indirectly the measured eigenvalues. For absolute values of a_2 ranging from 0 to 1 meV, the fit presented in the figure is preserved with $D=(14\pm 10)\times 10^{-5}$ meV. According to Eq. (4), it corresponds to $\omega=130\pm 60$ cm^{-1} for the radial vibration of the rotor.

Higher harmonics of the hindering potential affect the displayed results very little. The potential is therefore undetermined in regard to the angular energy barrier and the position and number of minima. This is illustrated in Fig. 3, where three different hindering potentials are displayed, which are perfectly compatible with the experimental information: (i) $a_1<0$ and $a_2=0$, (ii) $a_1<0$ and $a_2<0$, and (iii) $a_1<0$ and $a_2>0$. They show qualitative differences explained in the following.

Along the rotation path there are two different kinds of symmetry positions, the C_s positions, where the complex has a specular symmetry with respect to the plane containing the oxygen atom and its nearest neighbors, and the C_2 positions, where the complex is invariant under a rotation of 180° around an axis perpendicular to the Ge-Ge axis, passing through the oxygen atom. There are six equivalent C_s positions, separated by 60° from each other, and by 30° from the six C_2 positions. The first potential in Fig. 3 corresponds to a situation where one kind of symmetry position corresponds to the potential minima and the other kind to the maxima, $4a_1$ representing the energy barrier. The second potential displays local minima at both C_s and C_2 positions, but with different energy for the different positions, 12 local maxima appearing in between. The last potential shows 12 equivalent minima at no symmetry positions, separated by different maxima at each side, one at C_s and the other at C_2.

The different scenarios presented are compatible with the data, the discrimination among them being thus impossible on these grounds. The measurement of the splitting of the $m=\pm 6$ levels would give new qualitative information allowing the direct evaluation of $|a_2|$. There is an additional indetermination in ascertaining which ones of the symmetry positions correspond to minima or maxima. This information cannot be obtained with the experimental techniques used. See the next subsection for complementary theoretical information.

Recently, an additional absorption has been found by phonon spectroscopy[16] with an energy of 4.74 meV. If interpreted within the rotor model, it implies an unreasonably large value of $a_2=1.5$ meV, much larger than a_1. Another interpretation[16] assigns it to a radial excitation, which implies a small (≈ 10 meV) energy barrier along the radial direction. This is difficult to reconcile with the data and discussion presented in the following sections. Further experimental knowledge is needed to understand this point. It should be remembered, however, that the model discussed here represents quite a simplification, since many ingredients have been left out (accompanying rotation of Ge atoms, interaction of the O rotation with the vibrations of the center and with the phonons of bulk germanium, etc.), the agreement achieved still being remarkable.

An alternative to the nearly free oxygen rotation model discussed above would be a tunneling model,[17] representing a situation where the angular variation of the potential is much more pronounced, and where the quantum delocaliza-

tion of the oxygen is through hopping among the potential minima. For the sake of completeness, a tunneling analysis[18] has been performed for the three situations described above (the three potentials depicted in Fig. 3 for Ge:O_i), using tight-binding-like models for six and 12 positions. The main conclusion is that the three tunneling possibilities give a substantially worse fit of the energy levels than the nearly free rotation model.

It is important to stress that the qualitative differences between Si:O_i and Ge:O_i displayed in Fig. 2 have a clear manifestation in the different energy scales at which the low-energy excitations appear. The angular delocalization of oxygen in germanium gives rise to low lying rotation excitations with energies of the order of tenths of meV, which are essentially decoupled from the vibrational modes at an energy scale given by ω (of the order of 20 meV). In silicon, radial and angular excitations are nontrivially mixed in a common intermediate energy scale.

B. Ge rotation and isotope shifts

Natural silicon and germanium are made up of three and five isotopes, respectively. An isotope-shift study of the low-energy modes of Si:O_i has revealed only an effect of the mass of the O atom and the information has been used for the characterization of the center,[10,11,14] but there are no results of any kind in the Ge:O_i case. Isotope shifts in the Ge case can give important information for the understanding of the center as they can show how the germanium atoms rotate. So far, the implicit assumption has been that the rotation is mainly the same as the rotation of the free Ge_2O molecule, introducing always the reduced mass μ of such unit as the relevant mass. In the following a discussion is presented on that issue, showing that this picture is not necessarily correct. The expected isotope shifts of the rotor levels are presented, both for oxygen- and germanium-isotope substitutions, as important information to define this point.

The fit of the experimental data to a rotor model presented above does not give precise information on *what* is rotating. Obviously, the oxygen atom is involved in the rotation, but the assumption that only the oxygen atom rotates would be naive. It is clear that the neighboring germanium atoms are tightly bound by the rest of the crystal to quite defined positions, but they are not fixed, they can displace from those positions elastically. Even the simplest model of such a system (Ge-O-Ge with elastic restoring forces for the Ge atoms) has no simple analytical solution. Assuming that the Ge_2O unit is rotating freely is certainly dangerous and can be misleading.

If it is assumed that only oxygen rotates, the predictions are straightforward. The shift in the rotor levels due to an oxygen-isotope substitution with a change of mass Δm_O corresponds to the change of the rotor constant B (and the accompanying change of the D coefficient) due to the change of the momentum of inertia I [Eq. (3)] by

$$\Delta I = \Delta m_O R_a^2, \tag{8}$$

where

$$R_a = \sqrt{\frac{I}{m_O}} \tag{9}$$

is the ''apparent'' radius of rotation. There would be no shifts due to germanium substitutions.

A more realistic model should allow for a rotationlike motion of the Ge atoms neighboring O, and account for the interaction with phonons and localized vibrations. The latter can be treated in the phenomenological way proposed by Pajot and Cales,[13] with a renormalization of the germanium mass. The actual value for the renormalized mass m_{Ge}^* has to be obtained through fitting to experimental data. The interaction mass m' is defined as[13]

$$m_{Ge}^* = m_{Ge} + m'. \tag{10}$$

It should not be large compared with the masses themselves.

For the rotation of the germanium atoms, it is reasonable to assume that both rotate in phase (say for equal germanium masses). The fact that the germanium atoms are tied to the crystal makes the situation different from the free rotation of the Ge_2O molecule in vacuum, *the lowest energy for a given angular momentum being given by the in-phase rotation of oxygen and germanium*. In other words, the Ge atoms accompany the rotation of the O atom, instead of counter-rotating as they would do in a free molecule. However, both possibilities are discussed here for future comparison with experiment.

The moment of inertia for the rotating system is

$$I = m_O(R \pm r)^2 + 2m_{Ge}^* r^2, \tag{11}$$

where R is the distance of oxygen to the Ge-Ge axis (the relative coordinate) and r is the distance of the Ge-Ge axis to the rotation axis. The $\pm$ symbol stands for the two possibilities, $+$ for corotation (the three atoms rotating in phase), $-$ for counter-rotation. Equation (11) can be written as

$$I = m_O R^2 \xi, \tag{12}$$

with

$$\xi = \left(1 \pm \frac{r}{R}\right)^2 + \frac{2m_{Ge}^*}{m_O}\left(\frac{r}{R}\right)^2. \tag{13}$$

For corotation $\xi > 1$ for any r. For counter-rotation $\xi < 1$ when $r/R < 2m_O/(2m_{Ge}^* + m_O)$, and $\xi \geq 1$ otherwise. The minimum value of ξ is for $r/R = m_O/(2m_{Ge}^* + m_O)$.

Equation (12) can be given two interpretations to keep the simple rotor image. First, it gives the apparent radius, $R_a = R\sqrt{\xi}$, which shows how R_a changes when the germanium atoms rotate. Alternatively, an effective mass for oxygen can be defined as $m_O^{\text{eff}} = m_O \xi$ to absorb the effect of the Ge rotation. The effective mass is equal to the reduced mass (μ) of the Ge_2O molecule only in the particular case of counter-rotation with $r = m_O R/(2m_{Ge}^* + m_O)$, i.e., rotating around an axis containing the center of mass. As mentioned above, it is not expected that the molecule will rotate around the center of mass, but rather corotate around a different axis, and therefore the effective mass of oxygen is expected to be *larger* than the bare atomic mass, instead of smaller in the sense of the reduced mass.

These issues will be at least partially settled with isotope-shift measurements of the rotor levels. First, r can be readily determined by isotopic substitution of germanium. From Eq. (11),

TABLE I. Calculated isotope shifts (cm^{-1}) of the rotor energy levels, both for oxygen and germanium substitution, and for $r=0.10$ and 0.13 Å. Δm in amu.

	r (Å)	$l=1$	2	3	4	5
$\Delta m_O=2$	0.10	0.14	0.54	1.17	2.01	3.01
	0.13	0.12	0.47	1.02	1.77	2.65
$\Delta m^*_{Ge}=6$	0.10	0.02	0.06	0.14	0.24	0.35
	0.13	0.03	0.10	0.20	0.35	0.52

$$(\Delta I)_{Ge}=2r^2\Delta m^*_{Ge}. \tag{14}$$

The radius of rotation of the Ge atoms can be read from the slope of the plot of $(\Delta I)_{Ge}$ versus Δm^*_{Ge}. For small interaction mass m', the latter can be approximated by Δm_{Ge}. If m' is large, an alternative procedure would be more appropriate for isotopically pure samples: take $\Delta m^*_{Ge}=\chi\Delta m_{Ge}$, with χ defined by $m^*_{Ge}=\chi m_{Ge}$.

Oxygen substitution gives

$$(\Delta I)_O=(R\pm r)^2\Delta m_O, \tag{15}$$

which gives R, the O-Ge relative coordinate, except for the fact that either corotation or counter-rotation have to be assumed. An independent estimation of R will therefore ascertain between the two rotation possibilities (see below). For that purpose, the momentum of inertia obtained from experiment can be used to obtain a relation between R and r. From Eq. (11),

$$R=\sqrt{\frac{I-2m^*_{Ge}r^2}{m_O}}\mp r. \tag{16}$$

For the counter-rotating case (+), R changes only slightly, staying between 0.8 and 0.9 Å for values of r up to 0.2 Å. In the corotating case, R appreciably diminishes with r, from 0.85 Å for $r=0$, to 0.7 Å for $r=0.1$ Å, and to 0.4 Å for $r=0.2$ Å. The reduction is more pronounced the larger the mass renormalization of Ge. To get a feeling of the size of r, note that the center-of-mass counter-rotation assumption presumes a value of 0.1 Å.

Table I shows the expected isotope shifts calculated for the observed rotor spectral lines, for germanium ($\Delta m^*_{Ge}=6$ amu) and oxygen ($\Delta m_O=2$ amu) substitutions. The shifts are presented for two different r values, 0.10 and 0.13 Å (see below). Note that for larger r, the oxygen-isotope shifts are smaller while the germanium-isotope shifts are larger.

C. First-principles potential wells

The results presented in the preceding subsections are self-consistent, but there are points regarding the atomic configuration and nuclear potentials that the available experiments cannot answer. Complementary information is sought using first-principles total-energy calculations to study the potential for the nuclear motion. The calculations have been performed in the manner described elsewhere,[12] using a cluster-Hartree-Fock approximation. The electronic energy is calculated for different distances of the oxygen atom to the BC position along a perpendicular direction to the Si-Si or Ge-Ge axis. At each point, the first and second nearest neighbors of oxygen are carefully relaxed. This represents an adiabatic radial potential for the oxygen motion with respect to the Si/Ge atoms. It is a good approximation to the effective potential obtained from experiments, as discussed in the next subsection, and, in more detail, in Ref. 19. The calculations are performed for the C_s symmetry of the center. The Si(Ge) atoms nearest to O were relaxed along the original Si-Si (Ge-Ge) axis.

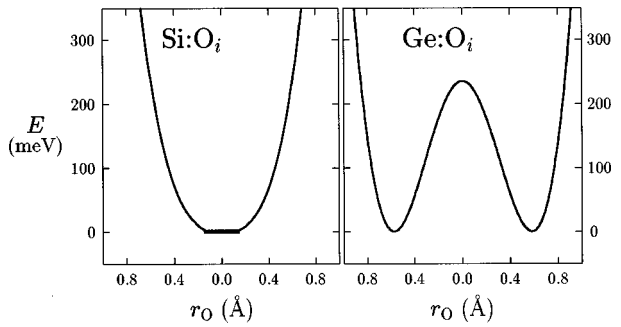

FIG. 4. Radial potential for the oxygen motion for Si:O_i and Ge:O_i obtained from first principles relaxing up to second nearest neighbors of oxygen for every point. There is a region in the Si:O_i case (Ref. 12) where the potential is flat within the limits given by the computational scheme, the maximum barrier being of the order of 1 meV. It is compatible with the potential in Fig. 3.

The resulting radial potentials are shown in Fig. 4 for both centers. Note the qualitatively different size of the barrier for the radial motion. In the Ge:O_i case it amounts to 235 meV, localizing the oxygen distance to BC around $r_O=0.58$ Å. The Si:O_i case displays a radial barrier of at most 1 meV.[12] These numbers provide additional support for the picture in Fig. 2. In the equilibrium geometry the Ge-O-Ge (Si-O-Si) angle is 140° (180°) and the Ge-O (Si-O) distance 1.70 Å (1.56 Å).

A simple calculation can be made that supports the difference in the potential barriers displayed in Fig. 4. Consider the Ge—O bonds of the Ge_2O unit as springs, with the Ge positions fixed and the O atom free to move. Let the disposition be such that the relaxed situation has a defined Ge-O-Ge angle, θ. Considering Hooke's law for the stretching of the springs, the barrier, i.e., the potential energy needed to push the O atom to the axis, is

$$E_B=kl^2[1-\sin(\theta/2)]^2, \tag{17}$$

where k is the stretching force constant, and l the length of the Ge—O bond. Taking $k=3.4\times10^5$ dyn/cm (see Sec. III A), $l=1.7$ Å, and $\theta=140°$, the barrier amounts to $E_B=220$ meV, quite in agreement with the 235 meV of the *ab initio* calculation. Doing the same for Si:O_i, with $k=4.8\times10^5$ dyn/cm, $l=1.56$ Å, and $\theta=168°$ (see the static potential in Ref. 11), the result for the barrier is $E_B<2$ meV, in accordance with the previous discussion for Si.

The radius $r_O=0.58$ Å obtained from the calculations for Ge:O_i corresponds to the R quantity defined in the preceding subsection. It is much smaller than the apparent radius $R_a=0.85$ Å obtained from a fixed-Ge interpretation of the rotor experimental data, and even smaller than the radius of 0.92 Å obtained[6] assuming the reduced mass of the Ge_2O

pseudomolecule. According to the discussion above, a value of R smaller than the apparent one indicates a coordinated rotation of O and Ge atoms, all in phase, against the previous belief of a rotation around the center of mass, i.e., Ge and O rotating in antiphase. Of course, there is an expected error in the theoretical estimate of R due to the approximations involved in the first-principles scheme. The 0.27 Å deviation, however, is too large to be accounted for by just numerical error. It has to be remembered that one of the main approximations of the scheme lies in the finite size of the cluster, its main shortcoming for this system being the lack of relaxations further than second nearest neighbors to oxygen. The system being under compressive stress, it is clear that the improvement of the calculation on this point would render an even smaller value of R.

Based on the formulas of the preceding subsection, $R=0.58$ Å implies a radius for the accompanying Ge rotations $r\approx 0.13$ Å. It is larger but of similar magnitude to the 0.1 Å presumed before (center-of-mass assumption). Even if the first-principles results could still give too short a radius, the deviation for R should be considerably smaller than 0.27 Å. See, for instance, the independent result of Laβmann[16] of $\theta=(138\pm 8)°$ obtained from uniaxial stress measurements, very similar to our 140°.

For the characterization of the ϕ dependence of the potential, additional first-principles calculations are performed at C_2 symmetry positions (30° away from the previous), and at an intermediate ϕ value between C_s and C_2. No significant difference in the relaxation of the neighboring atoms is observed. The lowest energy is found for the C_2 symmetry positions, the C_s position representing local minima, too, with barriers at the intermediate positions. This scenario corresponds to the second potential in Fig. 3. The numbers, however, are way too small: $E_{C_s}-E_{C_2}\approx 3\,\mu$eV, while the rotor analysis indicates rather 520 μeV. There are neither noise nor numerical problems in our computational scheme, but it involves certain approximations that by no means allow relying on such small energy scales. The main result in this respect is that the rotational barrier is negligible in accordance with what was obtained experimentally.

D. Quantum many-atom effects

The effective potentials obtained from fits to experiments and the adiabatic potentials obtained in the preceding subsection represent one-particle approximations to the real situation: the atoms move in a correlated fashion in a many-body potential. The usual situation, where the harmonic approximation applies for vibrations around a potential minimum, allows a decoupling of that potential. However, the drastic deviation of our systems from the harmonic behavior prevents such decoupling.

1. Si:O_i

On the grounds of the effective one-particle potential, it has been argued before[11,12] that Si:O_i has to be described in terms of a linear geometry, as displayed in Fig. 2. In this section we check that conclusion within the more realistic frame of the many-atom problem. Yamada-Kaneta, Kaneta, and Ogawa[11] include some interatom correlations by coupling the low-energy motions of oxygen to the high-energy stretching mode. The analysis presented here treats the O and neighboring Si atoms and their correlations on equal footing.

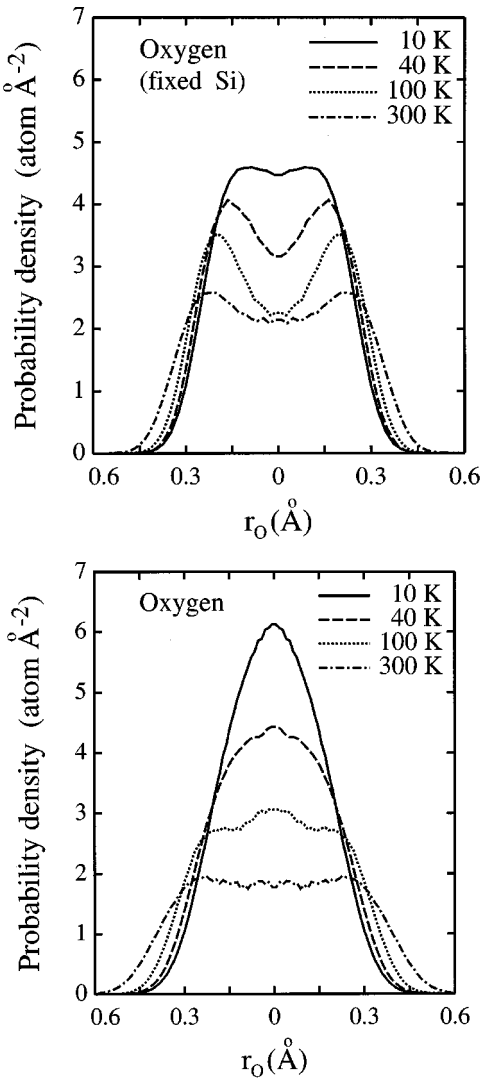

FIG. 5. Probability density $\rho(r_O)$ for the O nucleus obtained in the PIMC simulation at several temperatures. r_O is the distance from the impurity to the BC site. Top: the Si atoms were fixed at the positions of the absolute potential minimum. Bottom: the Si atom nearest neighbors to the impurity are allowed to move along the broken bond direction.

A theoretical study of the quantum dynamics of Si:O_i presents two major difficulties: (i) the computation of a realistic many-body potential, and (ii) the solution of the many-body problem. With respect to the first point, the Si-Si interaction is described by the Stillinger-Weber potential,[20] while the Si-O-Si interaction is modeled by an empirical three-body potential[21] that reproduces the main features of the Si:O_i defect, namely, its geometry (bond length, bond angle, and Si relaxations obtained from the first-principles calculations described above) and vibrations (A_{2u} and A_{1g} modes).

The many-particle quantum problem was solved by path-integral Monte Carlo (PIMC) simulations,[22] a technique that is appropriate for the study of equilibrium properties at finite temperatures. The results for the probability-density function $\rho(r_O)$ of the O nucleus are shown in Fig. 5 as a function of the temperature for two different constrained models. In the first model, the Si atoms are fixed at the relaxed positions

corresponding to the absolute minimum of the employed potential, with a Si-O distance of 1.53 Å and a Si-O-Si angle of 163°. The probability distribution is bimodal, the maximum probability density being found away from the BC site, and its symmetry corresponds to a nonlinear Si-O-Si arrangement. By allowing the Si nearest neighbors of the impurity to move along the (broken) bond direction, the $\rho(r_O)$ curve changes drastically and displays the symmetry expected for a linear arrangement of atoms, with its maximum at the BC site. This result shows that the geometry given by the minimum of the potential becomes meaningless for describing the properties of the impurity center, due to the zero-point motion of the impurity and the neighboring lattice atoms. This many-body treatment confirms the hypothesis made in a previous work[12] based on one-particle arguments, assigning a linear geometry to the center in spite of the puckered geometry that the potential would give.

2. Ge:O$_i$

In the Ge:O$_i$ case, the difference in energy scales involved in the rotation and vibrations of the center still permits the decoupling of both motions in the same way as for molecules in vacuum. Therefore the analysis presented in the preceding section together with the study of the higher-energy vibrations presented in the next section provide a qualitative and correct picture of the center. Therefore most of the correlated motions are understandable in easy terms. The only exception is the motion of the Ge atoms related to the O rotation, as pointed out in Sec. II B. Path-integral Monte Carlo simulations are useful to understand this point. A simplified model has been devised for the purpose, where the Ge lattice is kept fixed, allowing only the motion of O and its Ge nearest neighbors. In addition, both Ge atoms are only allowed to move in phase.

Preliminary results of PIMC simulations[23] indicate that the Ge atoms accompany the O rotation (corotate) instead of counter-rotating, which was the usual assumption (for instance, whenever the reduced mass of oxygen was used). This is concluded from the finding that $\langle \mathbf{r}_O \cdot \mathbf{r}_{Ge} \rangle > 0$, where the positions of O and Ge ($\mathbf{r}_O$ and $\mathbf{r}_{Ge}$, respectively) are taken with respect to the axis of rotation, i.e., the axis passing through the Ge positions in the ideal crystal. A more detailed analysis would be desirable and will be presented in the future,[23] but it is not expected to reveal new physics at the level of the present work.

III. THEORY OF VIBRATIONAL SPECTRA

A. Spectra and mode characterization

The microscopic models presented in the preceding section allow the calculation of the absorption spectra of these centers in the infrared range. A model dynamical-matrix calculation for the vibrations of a single O impurity in the infinite semiconductor is used for that purpose. The cluster-Bethe-lattice approach[24] is used to account for the infinite semiconductor system. A Born model is used for the dynamical matrix, the geometry being obtained from the *ab initio* results discussed above. Further details on the calculation scheme were presented elsewhere.[12] The central force constant (α) used for bulk Ge is 0.58×10^5 dyn cm^{-1} and the noncentral one (β) is 0.26×10^5 dyn cm^{-1} (Ref. 24). For the Ge_2O unit, a three-body bending force constant has been considered instead of the two-body noncentral force constant of the Born model. The reason is that the Born model is too simple for the adequate treatment of the puckered geometry, it cannot distinguish between the radial and the tangential vibrations (the latter corresponding to the rotation). The stretching (central) and bending force constants used are 3.41×10^5 dyn cm^{-1} and 0.31×10^5 dyn cm^{-1}, respectively.[25,26] The infrared absorption is calculated in absolute units (cm^{-1}) following Martínez and Cardona.[26]

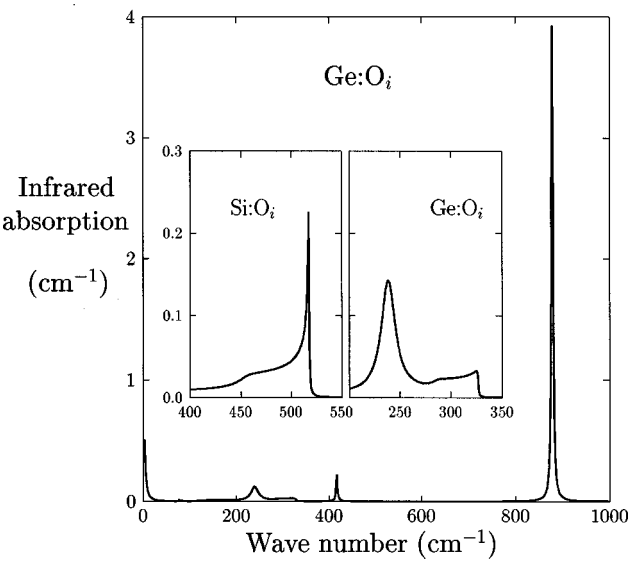

FIG. 6. Infrared-absorption coefficient calculated for Ge:O$_i$ for an oxygen concentration [O]=10^{18} cm^{-3}. The inset shows a magnification of the spectral region corresponding to the upper Ge phonon bands, compared with the equivalent region in Si:O$_i$.

The infrared-absorption spectrum obtained for Si:O$_i$ was already shown and discussed in a previous paper,[12] the comparison with the Ge case being presented below. The spectrum for Ge:O$_i$ is shown in Fig. 6. Four distinct features appear at 877, 416, 230, and 0 cm^{-1}. The latter corresponds to the free rotation of oxygen, zero frequency within this approximation.[27] The other three correspond to the ν_3 stretching, ν_1 bending, and ν_2 rocking modes of the Ge_2O unit, respectively[8] (see Fig. 7). It is worthwhile noting that this classification is well suited for the Ge:O$_i$ center due to

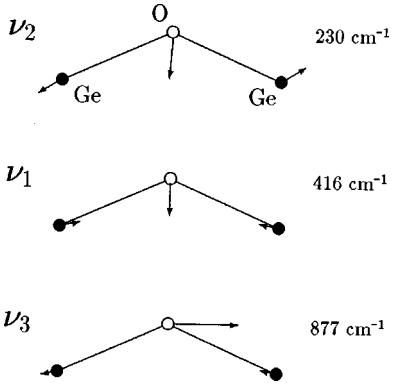

FIG. 7. Quantitative sketch of the relative motions of the atoms in the different modes of vibration of Ge:O$_i$.

its puckered geometry. For the Si:O_i center the appropriate classification[11,12] is shown in Fig. 1(b).

The asymmetric stretching mode at 877 cm^{-1} corresponds to the very well characterized main absorption peak at 860 cm^{-1} (Ref. 4), equivalent to the 1136 cm^{-1} peak for Si:O_i. The other two features (416 and 230 cm^{-1}) have never been directly observed in experiments. The ν_2 band appears as a resonance in the germanium continuum and corresponds to the radial vibration of the rotor. Indeed, the centrifugal distortion coefficient $D=4B^3/\hbar^2\omega^2$ in the hindered rotor model gives a value for ω of the magnitude of the frequency of this ν_2 mode [the exact value depends on the amplitude of the $\cos(12\phi)$ term]. The position of this ν_2 feature is not as well defined by our model as the others, being more sensitive to small changes in the dynamical matrix and/or geometry.

The mode at 416 cm^{-1} of Ge:O_i is of a similar origin as the 596 cm^{-1} mode of Si:O_i.[12] In the Ge case, however, there is an important O radial motion which is absent in the Si case. The difference lies on the puckering of the Ge_2O unit. In fact, both ν_1 and ν_2 modes involve the radial motion of the O atom. The difference between the two is found in the relative motion of the Ge neighbors, in phase with O for ν_2, antiphase for ν_1. The ν_1 vibration has not been observed experimentally because of the weakness of this feature, together with the fact that the infrared spectrum of crystalline germanium shows a two-phonon infrared absorption in this frequency range[28] that can hide the absorption of O_i at the usual concentration. Nevertheless, an O vibrational mode has been reported at 1270 cm^{-1} (Ref. 2) and it is a good candidate for a combination of the ν_1 symmetric mode with the asymmetric ν_3 stretch mode. It is the same effect as in Si:O_i, where the noninfrared active mode at 596 cm^{-1} combines with the asymmetric stretching one to give the 1751 cm^{-1} band.[29] These combination-mode assignments are soundly supported by the agreement of the isotope shifts predicted by the theory and the corresponding experimental results. These data have already been presented[12,14] for Si:O_i and are presented here for Ge:O_i (next subsection).

To obtain a quantitative measure of the atomic motions for the different modes, the displacement-displacement correlation functions

$$\langle \vec{u}_i \cdot \vec{u}_j \rangle = -\frac{\hbar\omega}{\pi} \lim_{\eta \to 0^+} \mathrm{Im}[\mathbf{G}_{ij}(\omega^2 + i\eta)] \qquad (18)$$

of atoms in the vicinity of the defect are shown in Fig. 8. $\vec{u}_i$ and $\vec{u}_j$ are the displacement vectors of atoms i and j. $\mathbf{G}_{ij}$ is the Green-function tensor corresponding to atoms i and j. The correlation functions shown confirm the assignments made above, and give the necessary information for a quantitative picture of the relative motions, as in Fig. 7. Also the mean square displacements of the atoms at the different vibrational modes are given in Table II.

The inset of Fig. 6 shows the infrared absorption near the upper edge of the bulk continuum for both Si:O_i and Ge:O_i. The figure shows remarkable differences between these two spectra. On the one hand, there is no spectral feature for Si:O_i that is equivalent to the 230 cm^{-1} mode of Ge:O_i. This is due to the fact that, in the Si case, the O radial motion is very soft due to the highly anharmonic potential, the associated mode mixing with the rotational motion in a lower-energy scale. For Ge both motions are well separated in different energy scales.

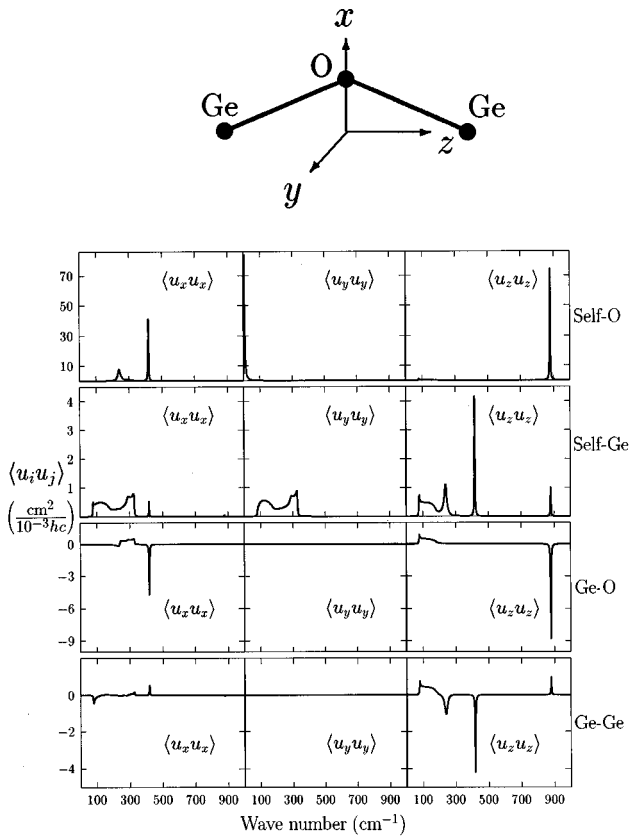

FIG. 8. Displacement-displacement correlation functions, $\langle u_i u_j \rangle(\omega)$ of oxygen, and neighboring germanium atoms in Ge:O_i.

On the other hand, the asymmetric resonance in Si:O_i at the phonon-band edge (517 cm^{-1}) is practically absent in Ge:O_i. This resonance appears due to the backbonding relaxation caused by the incorporation of oxygen. This relaxation is larger in silicon than in germanium. This assignment is confirmed by Fig. 9, which shows the displacement-displacement correlation functions between the silicon atoms forming the backbonds. These results show very explicitly the origin of the modes at 517 and 596 cm^{-1} in silicon. The mode at 517 cm^{-1} is a silicon optic mode (perpendicular to the defect axis), with a higher frequency due to the backbonding compression. The mode at 596 cm^{-1} is an optic mode (parallel to the axis) split off the band due to the presence of the stronger Si—O—Si bond in the semiconductor lattice.

TABLE II. Mean square displacements $\langle u_i^2 \rangle^{1/2}$ of the O and neighboring Ge atoms along the different directions (in pm). Axes defined in Fig. 8.

	O		Ge_1		Ge_2	
Mode	x	z	x	z	x	z
ν_2 (230 cm^{-1})	4.3	0.3	1.4	1.6	1.3	1.6
ν_1 (416 cm^{-1})	3.5	0.0	0.4	1.1	0.4	1.1
ν_3 (877 cm^{-1})	0.0	3.2	0.1	0.4	0.1	0.4

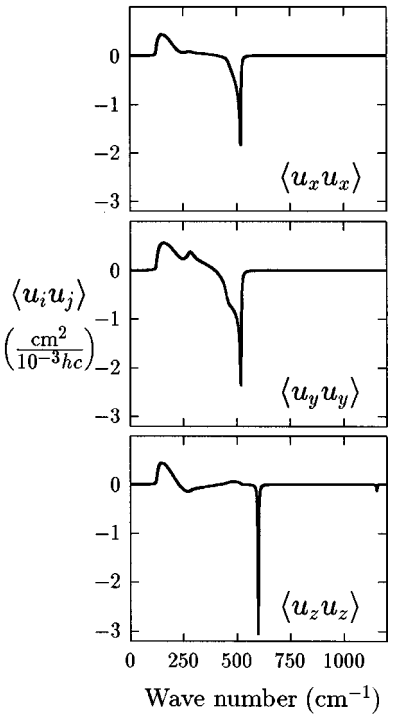

FIG. 9. Displacement-displacement correlation functions of the silicon atoms forming the backbonds in Si:O_i.

B. Isotope shifts

The method described above allows the calculation of shifts in the spectral features due to different isotope replacements. Shifts can be calculated for many isotopic-substitution combinations (changing O, changing one semiconductor neighbor, changing both neighbors, changing the host crystal atoms, etc.). Since only the masses of atoms change, implying no changes in the dynamical matrix, the isotope shifts obtained from theory have a high predictive power, and constitute an important check for the theory. The recent availability of isotopically pure or enriched semiconductor samples makes possible the measurement of these quantities.[8,30]

The isotope shifts for Si:O_i, both calculated and measured, were presented in a previous paper,[14] where the previous assignments and the existence of the A_{1g} symmetric stretching mode were confirmed experimentally. The corresponding results for Ge:O_i are presented in the next section. As a previous check on the theory, in Fig. 10 the isotope shifts of the ν_3 mode are shown for ^{18}O for the different combinations of Ge neighbors. They are compared with the experimental results of Mayur *et al.*,[8] showing satisfactory agreement.

IV. GERMANIUM-ISOTOPE-SHIFT MEASUREMENTS

A. Experimental details

Natural germanium is a mixture of ^{70}Ge (20.5%), ^{72}Ge (27.4%), ^{73}Ge (7.8%), ^{74}Ge (36.5%), and ^{76}Ge (7.8%). The Ge-isotope-shift (IS) measurements have been performed by infrared absorption near liquid helium temperature (LHeT). We report here the results on the asymmetric stretch (ν_3) mode and on what has been ascribed to the combination of this mode with the symmetric ν_1 mode of O_i [see Fig. 1(a)]. In natural Ge:O, the ν_3 transitions are sharp at LHeT, with a full width at half maximum (FWHM) near 0.03 cm^{-1} or about 4 μeV. By comparison the combination mode is about 350 times broader under the same conditions. This fact explains why, if it is possible to measure a Ge IS of ν_3 in natural germanium, this is not possible for the combination mode. Thus the Ge IS's of the combination mode have been measured in samples enriched with one isotope to concentrations larger than 80% (quasimonoisotopic or qmi samples). The different kinds of samples used are listed below.

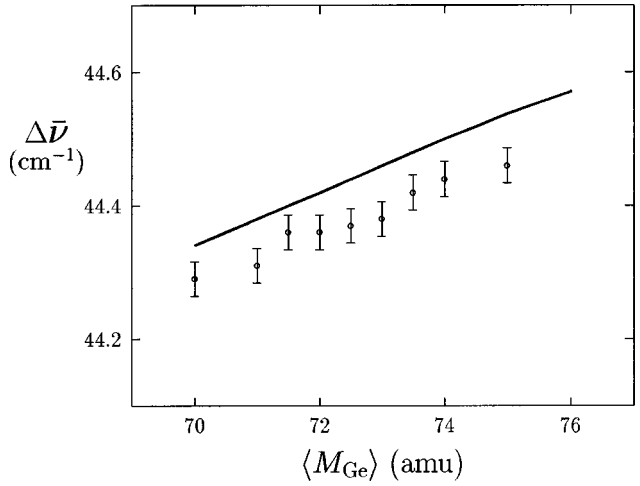

FIG. 10. ^{18}O-isotope shift of the ν_3 stretching mode of Ge:O_i for varying average mass of the Ge nearest neighbors to O. The line plots the theoretical results, the symbols show the experimental results of Mayur *et al.* (Ref. 8).

Two natural Ge:O samples were grown at Métallurgie Hoboken Overpelt and another, initially O-free, was diffused with oxygen for 14 days at 850 °C and cooled rapidly at room temperature at the University of Paderborn (Germany). One qmi ^{74}Ge:O Czochralski sample and one ^{76}Ge:O Bridgman sample have been grown at the University of Kiev (Ukraine). ^{70}Ge, ^{73}Ge, ^{74}Ge, and ^{76}Ge samples doped with oxygen have been grown by the vertical Bridgman method at the Lawrence Berkeley National Laboratory.[31]

The absorption was measured at 1.6 or 6 K with a BOMEM DA3+ Fourier transform infrared spectrometer with a unapodized spectral resolution of 0.013 cm^{-1} (ν_3) or with a resolution of 2 cm^{-1} (combination mode).

B. Results and discussion

The frequency of the feature near 860 cm^{-1} is due to the ν_3 mode. Its fine structure at low temperature comes from the combination of this mode with the nearly free rotation of the O atom about the Ge-Ge axis as depicted in Fig. 2 (the accompanying motion of the Ge atoms is disregarded). To simplify, it can be described by some kind of vibration-rotation spectrum of a pseudomolecule, with individual levels labeled $|v_3,l\rangle$. The situation here bears some similarity to the vibration-rotation spectrum of a diatomic molecule. The transitions observed take place between $|0,l\rangle$ and $|1,l\rangle$ states. Considering the experimental positions of the rotational states given in Fig. 3 and the fact that 6 K corresponds to a thermal energy of 0.5 meV, the four vibration-rotation

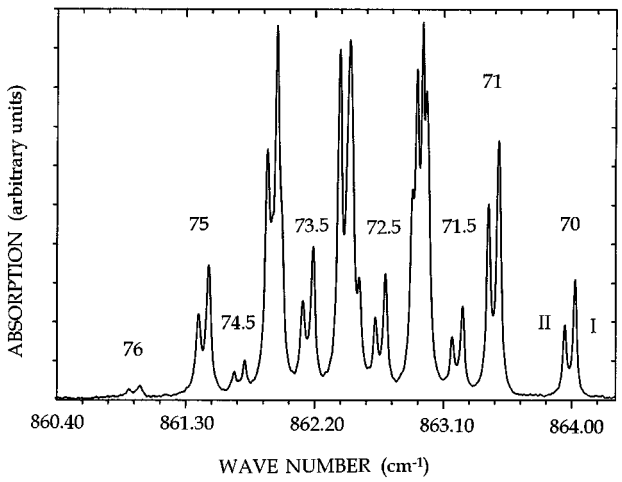

FIG. 11. Overall absorption at 1.6 K of the ν_3 mode in natural germanium. The characteristic doublets (lines I and II) due to the eight single combinations are clearly seen (Ge mass or average mass indicated). The three largest features, showing saturation, are due to two or three combinations with the same average Ge mass. Note the small intensity of the $^{76}Ge_2O$ combination. The average I–II spacing is 0.070 cm^{-1}.

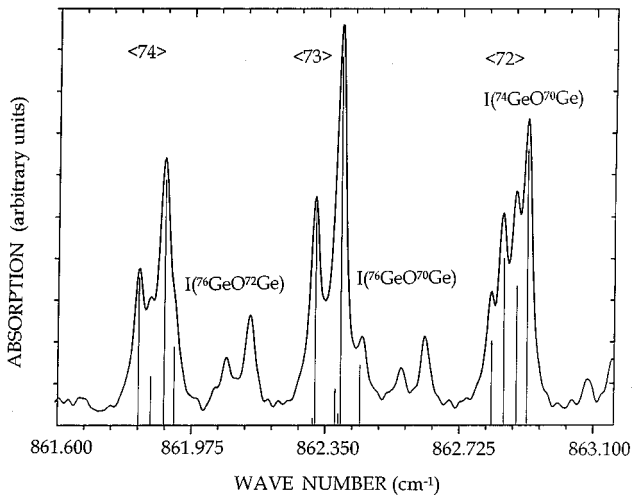

FIG. 12. Partial view at 1.6 K of the ν_3 mode absorption in a natural germanium sample with five times less oxygen than in Fig. 11. It shows more accurately the features due to average masses (AM's) 72, 73, and 74. The bars represent intensities calculated from the isotopic abundances. They are scaled to the observed intensities of lines I and II of $^{70}GeO^{72}Ge$, taken as references. For each AM, the label is for line I of the combination with the highest frequency. The ordering of the other components is, for AM=72, I($^{72}Ge_2O$), II($^{74}GeO^{70}Ge$), and II($^{72}Ge_2O$); for AM=73, I($^{74}GeO^{72}Ge$), I($^{73}Ge_2O$), II($^{76}GeO^{70}Ge$), II($^{74}GeO^{72}Ge$), and II($^{73}Ge_2O$); for AM=74, I($^{74}Ge_2O$), II($^{76}GeO^{72}Ge$), and II($^{74}Ge_2O$).

lines observed at 6 K are ascribed to transitions with $l=0$, ±1, ±2, and ±3. These transitions have been labeled I, II, III, and IV in this order.[8] It must be pointed out that the weak line IV has been detected for the first time in qmi germanium.[5] At 1.6 K, the reduction of the thermal energy depopulates the $|0,2\rangle$ and $|0,3\rangle$ levels, so that only lines I and II are observed and the 15 combinations of the five isotopes of natural Ge give 30 lines within a spectral range of three wave numbers. The spectrum of Fig. 11 shows indeed that about 25 lines can be resolved (this spectrum shows saturation effects for the most intense lines in order to see clearly the weak $^{76}Ge_2O$ combination).

In the linear approximation, the frequency of an asymmetric isotopic substitution YXY_i of a symmetric XY_2 molecule is taken as the mean of the frequencies of YXY and of Y_iXY_i. For the cases where the mean could be calculated accurately, it has been found that the deviation from the experimental value was indeed very small. In Ge, different Ge_2O isotopic combinations can have the same average Ge mass (AM) and this is the case for masses 72, 73, and 74, but they are found to vibrate at slightly different frequencies. Figure 12 shows a portion of the vibration rotation of ν_3 in natural Ge at 1.6 K where this can be seen. For the group of lines corresponding to AM=$\langle 72\rangle$, four components are resolved, which compare reasonably with (i) the relative intensities predicted for $^{74}GeO^{70}Ge$ and $^{72}Ge_2O$ (0.1500 and 0.075, respectively) and (ii) the relative intensities of lines I and II at 1.6 K. The fit shows that the highest frequency is for the asymmetric configuration. For $\langle 73\rangle$, six lines are expected, corresponding to $^{73}Ge_2O$, $^{74}GeO^{72}Ge$ and $^{76}GeO^{70}Ge$, but the ratio of the intensities of the $^{73}Ge_2O$ and $^{74}GeO^{72}Ge$ combinations is 0.03 while the frequency shift is estimated to be ~0.015 cm^{-1}. In this case, only the components due to $^{74}GeO^{72}Ge$ and $^{76}GeO^{70}Ge$ can be observed, but the mass difference between ^{70}Ge and ^{76}Ge is such that II($^{76}GeO^{70}Ge$) nearly coincides with I($^{74}GeO^{72}Ge$), explaining the observation of only three components. There again, the expected intensities are relatively well reproduced. The situation for $\langle 74\rangle$ is similar to the one for $\langle 72\rangle$, but the relative intensities preclude the resolution of separation of I($^{76}GeO^{72}Ge$) from I($^{74}Ge_2O$). Table III summarizes the shift measured for different Ge-isotope combinations with the same AM, compared with the values calculated as in Sec. III.

In natural silicon (^{28}Si: 92.2%, ^{29}Si: 4.7%, and ^{30}Si: 3.1%), the $^{29}Si_2O$ and $^{28}SiO^{30}Si$ combinations both correspond to AM=$\langle 29\rangle$. At 6 K, for the ν_3 mode, each combination gives only one line with a FWHM of 0.6 cm^{-1}. It is not possible to observe the $^{29}Si_2O$ line because its intensity is about 0.04 times the one of $^{28}SiO^{30}Si$ and the frequencies are very close. It is, however, possible to obtain an accurate value (1132.56 cm^{-1}) of the position of the $^{29}Si_2O$ line from those of $^{28}Si_2O$ and $^{28}SiO^{29}Si$ using the linear approximation. As for germanium, it is found that for the same AM, the frequency of the symmetric mode in silicon is slightly less than that of the asymmetric one (1132.72 cm^{-1} for $^{28}SiO^{30}Si$).

In the natural germanium samples, the total ^{70}Ge-^{76}Ge IS of the ν_3 mode measured on lines I and II at 1.6 K is (2.960 ± 0.004) cm^{-1} at LHeT. This value is significantly different from (2.939 ± 0.006) cm^{-1} derived for the same lines from Ref. 8 and measured on qmi germanium samples. One reason for this is that in qmi ^{70}Ge and ^{76}Ge, the ν_3 lines are slightly shifted towards lower and higher frequencies, respectively, when compared with natural germanium. This effect is attributed to the frequency dependence of the coupling of the germanium three-phonon background with the ν_3 mode. This is also probably the reason why in natural germanium, the FWHM's increase from $^{70}Ge_2O$ to $^{76}Ge_2O$.

TABLE III. Observed and calculated isotope shifts of the ν_3 mode (in cm^{-1}) due to different Ge-isotope combinations at O neighboring sites, for the same average mass (in amu).

		Δ(I)		Δ(II)
	$\langle M_{Ge}\rangle$	Expt.	Theor.	Expt.
$^{72}GeO^{74}Ge$-$^{73}Ge_2O$	73	0.006	0.010	
$^{72}GeO^{76}Ge$-$^{74}Ge_2O$	74	0.031	0.040	0.032
$^{70}GeO^{74}Ge$-$^{72}Ge_2O$	72	0.033	0.044	0.032
$^{70}GeO^{76}Ge$-$^{72}GeO^{74}Ge$	73	0.063	0.084	

Except for the above difference, which has a physical explanation and for the same frequency attributed to combinations with the same AM in Ref. 8, the agreement on the ISs on natural germanium presented here and those of Ref. 8 can be considered as good.

The behavior of the numbers in Table III can be rationalized in the following way. Consider the mass deviation, $\Delta M_{Ge}=(M_{Ge_1}-M_{Ge_2})/2$, as a small parameter such that the frequency of a mode can be written as

$$\nu(\Delta M_{Ge})=\nu_0+C(\Delta M_{Ge})^2, \tag{19}$$

where ν_0 is the frequency for equal masses, and C a constant. A linear term cannot exist (assuming smooth behavior) since the frequency of the mode cannot depend on which one of the Ge atoms is heavier, i.e., it cannot depend on the sign of ΔM_{Ge}.

According to Eq. (19), the shifts shown in Table III should be the following:

$$\nu(^{72}GeO^{74}Ge)-\nu(^{73}Ge_2O)=C,$$

$$\nu(^{72}GeO^{76}Ge)-\nu(^{74}Ge_2O)=4C,$$

$$\nu(^{70}GeO^{74}Ge)-\nu(^{72}Ge_2O)=4C,$$

$$\nu(^{70}GeO^{76}Ge)-\nu(^{72}GeO^{74}Ge)=9C-C=8C.$$

The description is quite accurate both for the experimental and for the theoretical numbers, the constant C being 0.008 cm^{-1}/amu^2 and 0.010 cm^{-1}/amu^2 for experiments and theory, respectively. For silicon, a value of about 0.16 cm^{-1}/amu^2 is found experimentally for C.

The feature at 1270 cm^{-1} was first reported by Kaiser and attributed to an O-related vibration.[2] Its peak absorption is much weaker than the ν_3 absorption, as seen from Fig. 13. The FWHM is about 10 cm^{-1} and no fine structure is observed at high resolution. The measurement of the Ge IS is thus clearly not possible in natural Ge. Different qmi Ge:O samples have then been used for this determination. Figure 14 shows this mode for qmi ^{70}Ge, ^{74}Ge, and ^{76}Ge. The effect is not so spectacular as for the ν_3 mode, but the ^{70}Ge-^{76}Ge IS is nonetheless four times larger. The FWHM of the mode in qmi Ge seems comparable to the one in natural Ge, except for ^{70}Ge, but the signal-to-noise ratio for this spectrum is poor. Thus, this mode seems to be homogeneously broadened.[32] Assuming that the 1270 cm^{-1} mode is a $(\nu_1+\nu_3)$ combination, one can derive from the experimental results the Ge ISs of the ν_1 mode and compare them with the calculations. This is presented in Table IV and the consistency of the results further supports the attribution. The ν_1 mode has been looked for in the spectral region where it is predicted to vibrate without positive result.

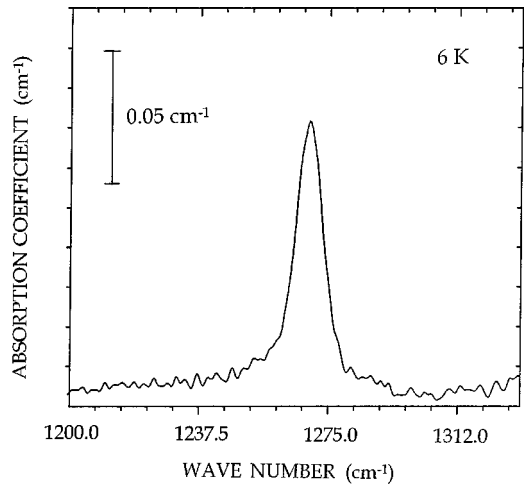

FIG. 13. Absorption at 6 K of the 1260 cm^{-1} mode in natural germanium with three times more oxygen than in Fig. 11. One abscissa division is 7.5 cm^{-1} compared to 0.075 cm^{-1} in Fig. 12.

V. CONCLUSIONS

$Ge:O_i$ has been thoroughly studied both experimentally and theoretically, achieving a fair understanding of the microscopic structure and the dynamics of this center. The experiments performed were based on infrared absorption spectroscopy of isotopically pure samples. The theory included (i) a hindered rotor model for the low lying excitations of the center, (ii) first-principles calculations for the potential the atoms are moving in due to the electrons, (iii) path-integral Monte Carlo simulations for the atom-atom correlation effects, and (iv) a model calculation of the infrared-absorption spectra. The $Ge:O_i$ center has been compared with $Si:O_i$, providing some new theoretical information for the latter concerning the quantum delocalization of the O atom.

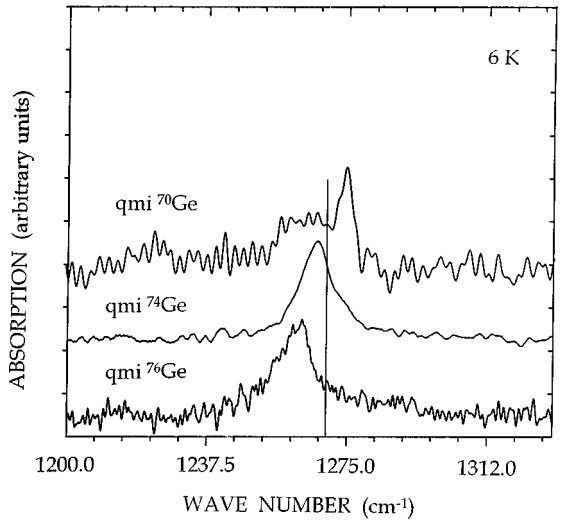

FIG. 14. Absorption at 6 K of the combination modes in different qmi Ge samples showing the Ge-isotope shift. The bar indicates the position of the mode in natural Ge.

TABLE IV. Observed and calculated spectrum modes for $^{70}Ge_2{}^{16}O$ (cm^{-1}), and corresponding isotope shifts. Numbers in brackets are determined indirectly. Numbers in parentheses come from the high resolution data of Ref. 8.

	ν_1		ν_3			$\nu_1+\nu_3$	
	Expt.	Theor.	Expt.		Theor.	Expt.	Theor.
$^{70}Ge_2O$	[411.2]	415.82	863.8	(863.92)	877.48	1275	[1293.30]
$^{73}Ge_2O$	[4.5]	4.15	1.5	(1.54)	2.03	5.9	[6.18]
$^{74}Ge_2O$	[6.4]	5.47	2.0	(2.02)	2.68	8.3	[8.15]
$^{76}Ge_2O$	[8.9]	7.96	3.0	(2.94)	3.92	11.9	[11.88]
Natural Ge	[4.3]	3.63	1.5		1.78	5.7	[5.41]

The main conclusion is presented in Fig. 2. In both cases ($Ge:O_i$ and $Si:O_i$) the O atom, after breaking the original semiconductor-semiconductor bond, quantum delocalizes around the bond-center region. The character of that delocalization and of the associated dynamics, however, is very different for the two centers. For $Ge:O_i$ the delocalization is in an annulus around BC, the dynamics being rotational. For $Si:O_i$ the delocalization has its maximum probability density at the BC site, giving rise to an essentially linear disposition of the center, the low-energy dynamics being that of very anharmonic vibrations around that position.

A detailed analysis of the rotation in the $Ge:O_i$ center has been presented. Besides the information obtained about the hindered rotation dynamics and its connection with low-frequency vibrations, the remaining open questions have been pointed out and the ways to answer them have been proposed. In particular, the picture of the Ge_2O unit rotating around its center of mass has been revised, and an alternative has been proposed where the whole unit rotates in phase around an external axis.

The infrared spectral features of the $Ge:O_i$ center have been revised. The stretching ν_3 vibrational mode at 860 cm^{-1} is well known and characterized. The shift of this feature with the change of oxygen nearest neighbor isotopes has been observed and characterized. The other vibrations which are expected, ν_1 and ν_2, have not been directly observed yet. Theory gives a weak ν_1 absorption at 416 cm^{-1}. New experimental data on isotope shifts of the combination mode at 1270 cm^{-1} confirm that prediction.

The ν_2 mode would be the lowest vibrational mode of the center and should give a weakly infrared active resonance in the Ge inactive phonon continuum. The position of this feature cannot be ascertained with precision and may lie between 230 cm^{-1} and 100 cm^{-1}, but clearly above the low-energy rotational modes, which are in the range of a few cm^{-1}.

ACKNOWLEDGMENTS

We acknowledge interesting discussions with K. Laβmann, and communication of his results prior to publication. This work has been supported by the DGICYT of Spain through Grant No. PB92-0169, by the European Community INTAS Project No. 93-320, and by the U.S. National Science Foundation under Contract No. DMR94-17763.

[1] B. Pajot, in *Oxygen in Silicon*, edited by F. Shimura, Semiconductors and Semimetals Vol. 42 (Academic Press, New York, 1994), and references therein.

[2] W. Kaiser, J. Phys. Chem. Solids **23**, 255 (1962).

[3] J. W. Corbett, R. S. McDonald, and G. D. Watkins, J. Phys. Chem. Solids **25**, 873 (1964).

[4] B. Pajot and P. Clauws, in *Proceedings of the 18th International Conference on the Physics of Semiconductors*, edited by O. Engström (World Scientific, Singapore, 1987), p. 911.

[5] L. I. Khirunenko, V. I. Shakostov, V. K. Shinkarenko, and F. M. Vorobkalo, Fiz. Tekh. Poluprovodn. **24**, 1401 (1990) [Sov. Phys. Semicond. **24**, 663 (1990)].

[6] M. Gienger, M. Glaser, and K. Laβmann, Solid State Commun. **86**, 285 (1993).

[7] A. Lizón-Nordström and F. Ynduráin, Solid State Commun. **89**, 819 (1994).

[8] A. J. Mayur, M. D. Sciacca, M. K. Udo, A. K. Ramdas, K. Itoh, J. Wolk, and E. E. Haller, Phys. Rev. B **49**, 16 293 (1994).

[9] E. Artacho and F. Ynduráin, Mater. Sci. Forum **196-201**, 103 (1995).

[10] D. R. Bosomworth, W. Hayes, A. R. L. Spray, and G. D. Watkins, Proc. R. Soc. London, Ser. A **317**, 133 (1970).

[11] H. Yamada-Kaneta, C. Kaneta, and T. Ogawa, Phys. Rev. B **42**, 9650 (1990).

[12] E. Artacho, A. Lizón-Nordström, and F. Ynduráin, Phys. Rev. B **51**, 7862 (1995); E. Artacho and F. Ynduráin, in *Proceedings of the 22nd International Conference on the Physics of Semiconductors*, edited by D. J. Lockwood (World Scientific, Singapore, 1995), p. 2459.

[13] B. Pajot and P. Cales, in *Oxygen, Carbon, Hydrogen, and Nitrogen in Crystalline Silicon*, edited by J. C. Mikkelsen, Jr. *et al.*, MRS Symposia Proceedings No. 59 (Materials Research Society, Pittsburgh, 1986), p. 39.

[14] B. Pajot, E. Artacho, C. A. J. Ammerlaan, and J. M. Spaeth, J. Phys., Condens. Matter. **7**, 7077 (1995).

[15] G. Herzberg, *Infrared and Raman Spectra of Diatomic Molecules* (D. Van Nostrand Company, Inc., Princeton, 1945), p. 104.

[16] K. Laβmann, Mater. Sci. Forum **196-201**, 1563 (1995).

[17] E. Artacho and L. M. Falicov, Phys. Rev. B **43**, 12 507 (1991).

[18] E. Artacho (unpublished).

[19] R. Ramírez, C. P. Herrero, E. Artacho, and F. Ynduráin, J. Phys., Condens. Matter. **9**, 3107 (1997); R. Ramírez, C. P. Herrero, and E. Artacho, in *Proceedings of the 23rd International Conference on the Physics of Semiconductors*, edited by M. Scheffler and R. Zimmermann (World Scientific, Singapore, 1996), p. 2613.

[20] F. H. Stillinger and T. A. Weber, Phys. Rev. B **31**, 5262 (1985).

[21] The analytical form of the employed potential is given in Ref. 19. The potential parameters are $k=35.6$ eV Å^{-2}, $r_e=1.629$ Å, $s_1=1.45$ eV, $s_2=-0.6$ eV, $l_1=4.5$ eV, and $\alpha_e=168°$, where the labels are taken from Ref. 19. The potential between the Si atoms forming the bond broken by oxygen was modified by adding an additional harmonic interaction $\frac{1}{2}k_s(r-r_s)^2$, with $k_s=6$ eV Å^{-2}, and $r_s=3.049$ Å.

[22] M. J. Gillan, in *Computer Modelling of Fluids, Polymers, and Solids*, edited by C. R. A. Catlow, S. C. Parker, and M. P. Allen (Kluwer, Dordrecht, 1990).

[23] C. P. Herrero (unpublished).

[24] F. Ynduráin, Phys. Rev. Lett. **37**, 1062 (1976).

[25] R. A. Barrio, F. L. Galeener, and E. Martínez, Phys. Rev. B **31**, 7779 (1985).

[26] E. Martínez and M. Cardona, Phys. Rev. B **28**, 880 (1983).

[27] The model dynamical matrix introduced in this section does not describe the potential that hinders O rotation, and therefore there is a free motion (the O rotation) that results in a zero-frequency mode in the harmonic treatment presented at this point.

[28] R. Tubino, L. Piseri, and G. Zerbi, J. Chem. Phys. **56**, 1022 (1972); K. Winer and M. Cardona, Phys. Rev. B **35**, 8189 (1987), and references therein.

[29] B. Pajot, H. J. Stein, B. Cales, and C. Naud, J. Electrochem. Soc. **132**, 3034 (1985).

[30] E. E. Haller, Semicond. Sci. Technol. **5**, 319 (1990); H. D. Fuchs, P. Etchegóin, M. Cardona, K. Itoh, and E. E. Haller, Phys. Rev. Lett. **70**, 1715 (1993); E. E. Haller, Appl. Phys. Rev., J. Appl. Phys. **77**, 2857 (1995).

[31] K. Itoh, W. L. Hansen, E. E. Haller, J. W. Farmer, V. I. Ozhogin, A. Rudnev, and A. Tikhomirov, J. Mater. Res. **8**, 1341 (1993).

[32] M. Cardona, P. Etchegoin, H. D. Fuchs, and P. Molinàs-Mata, J. Phys., Condens. Matter. **5**, A61 (1993).